A new method to determine the aerosol optical properties from multiple wavelength O_4 absorptions by MAX-DOAS observation

Chengzhi Xing[1], Cheng Liu[1, 2, 3, 7*], Shanshan Wang[4, 5*], Qihou Hu[3], Haoran Liu[1], Wei Tan[3], Wenqiang Zhang[3, 6], Bo Li[1], Jianguo Liu[2, 3]

[1]School of Earth and Space Sciences, University of Science and Technology of China, Hefei, 230026, China
[2]Center for Excellence in Regional Atmospheric Environment, Institute of Urban Environment, Chinese Academy of Sciences, Xiamen, 361021, China
[3]Key Lab of Environmental Optics & Technology, Anhui Institute of Optics and Fine Mechanics, Chinese Academy of Sciences, Hefei, 230031, China
[4]Shanghai Key Laboratory of Atmospheric Particle Pollution and Prevention (LAP[3]), Department of Environmental Science and Engineering, Fudan University, Shanghai, 200433, China
[5]Shanghai Institute of Eco-Chongming (SIEC), No.3663 Northern Zhongshan Road, Shanghai, 200062, China
[6]School of Environmental Science and Optoelectronic Technology, University of Science and Technology of China, Hefei, 230026, China
[7]Anhui Province Key Laboratory of Polar Environment and Global Change, USTC, Hefei, 230026, China

[*]*Correspondence to*: Shanshan Wang (shanshanwang@fudan.edu.cn) and Cheng Liu (chliu81@ustc.edu.cn)

Abstract. Ground based Multi-AXis Differential Optical Absorption Spectroscopy (MAX-DOAS) observation was carried out from November 2016 to February 2017 in Beijing, China to measure the O_4 absorptions in UV and visible bands and further to illustrate its relationship with aerosol optical properties (AOPs) under different the weather types. According to relative humidity, visibility and $PM_{2.5}$, we classified the observation periods into clear, light-haze, haze, heavy-haze, fog and rainy five different weather conditions. There are obvious differences for measured AOPs under different weather conditions, especially scattering coefficient (σ_{sca}) and absorption coefficient (σ_{abs}). It was also found that both the O_4 Differential Slant Column Densities (DSCDs) at UV and visible bands varied in the order of clear days > light-haze days > haze days > heavy-haze days > fog days. The correlation coefficients (R^2) between O_4 DSCDs at 360.8 and 477.1 nm mainly varied in the order of clear days > light-haze days > haze days > heavy-haze days. Based on the statistics of O_4 DSCDs at elevation angle 1° with the corresponding linear regression between UV and visible bands of segmental periods, the relationships between O_4 DSCDs and AOPs were established. It mainly should be clear or light-haze days when the correlation slope is greater than 1.0, correlation coefficient (R^2) greater than 0.9 and O_4 DSCDs mainly greater than 2.5×10^{43} molec cm^{-2}. Meanwhile, σ_{sca} and σ_{abs} are less than 45 and 12 Mm^{-1}, respectively. For haze or heavy-haze days, the correlation slope is less than 0.6, R^2 less than 0.8 and O_4 DSCDs mainly less than 1.3×10^{43} molec cm^{-2}, under which σ_{sca} and σ_{abs} are mainly located at 200-900 and 20-60 Mm^{-1}. Additionally, the determination method was well validated based on another MAX-DOAS measurement at Gucheng from 19 to 27 November 2016. For more precise and accurate inversion of AOPs, more detailed look-up tables for

O_4 multiple wavelength absorptions need to be developed. Furthermore, the vertical spatial-resolved aerosol scattering and absorption information is worthy of being expected by using DSCDs at different elevation angles.

1 Introduction

Atmospheric aerosols influence the radiative budget by scattering and absorbing solar radiation directly. It also affects the global climate change, cloud formation, regional air quality and human health (Seinfeld and Pandis, 2006; Kim and Ramanathan, 2008; Karanasiou et al., 2012; Levy et al., 2013; Viana et al., 2014). It is important to get a comprehensive knowledge on the spatial distributions, temporal variations of aerosol loading and Aerosol Optical Properties (AOPs). Different aerosol types behave obviously different optical properties. For example, Black Carbon (BC) aerosols are characterized by the strong light absorption. Recent studies indicated that it can heat the air, and contributes to global warming (Ramanathan et al., 2007; Galdos et al., 2013; Ramana et al., 2010; Fyfe et al., 2013; Allen et al., 2012). It can also change the atmospheric temperature vertical profile, causing the variations of the planetary boundary layer (PBL) structure (Ding et al., 2016; Wilcox et al., 2016; Wang et al., 2018). However, dust aerosol and some heterogeneous-reaction secondary aerosols, playing an important role during the pollution episode in China, are mainly based on scattering optical characteristics. (Huang et al., 2014; Wang et al., 2018).

Measurements of AOPs, e.g. Aerosol Extinction Coefficient (AEC), Aerosol Optical Depth (AOD), Single Scattering Albedo (SSA), asymmetry factor and Angstrom Exponent, could provide more comprehensive information for a better understanding of the role of aerosols in atmospheric processes. AOD is an important parameter to evaluate the ability of aerosol particles to attenuate the solar radiation, which is defined as the integration of AEC from surface to the top of atmosphere. The AE is the sum of aerosol scattering and absorption coefficients. Moreover, SSA is defined as the ratio of scattering efficiency to the total extinction, which is dominant intensive parameter determining aerosols direct radiative forcing. The asymmetric factor is used to evaluate the aerosol forward scattering ability, while the Angstrom is a parameter to evaluate the aerosol particle size. Previous measurements of AOPs indicated that different aerosol types (such as biomass burning, urban-industrial, dust and sea-salt aerosols) exhibit significant differences in optical properties. The differences of the optical properties of these kinds of aerosols are used to clarify the mechanisms of aerosol radiative forcing (Dubovik et al., 2001). For biomass burning aerosol, the Angstrom exponent is mainly distributed between 1.1 and 2.1 at wavelength bands of 440 – 870 nm and SSA mainly ranging from ~0.88 to 0.99 at 440 nm (Eck et al., 2003; Bergstrom et al., 2007; Weinzierl et al., 2017). The SSA of urban-industrial aerosol tend to be ~0.95 in cleaner condition and ~0.85 in industrially condition, respectively (Liousse et al., 1996; Remer and Kaufman, 1998; Garland et al., 2009; He et al., 2009; Shen et al., 2018). Dust exhibits a SSA ~0.92 to 0.93 in the blue spectral range at 440 nm, but ~0.96 - 0.99 in longer wavelength greater than 550 nm (Kaufman et al., 2001; Dubovik et al., 2001; Bergstrom et al., 2007; Weinzierl et al., 2017). The SSA in oceanic aerosol is mainly greater than 0.97 due to the existing of sea-salt and water soluble particles with high relative humidity (Tanré et al., 1999; Dubovik et al., 2001; Hess et al., 1998; Eck et al., 2005).

Multi-AXis Differential Optical Absorption Spectroscopy (MAX-DOAS) remote sensing is an effective tool for atmospheric aerosol measurements based on O_4 molecular ultraviolet-visible light absorption (Platt and Stutz, 2008). O_4 is the collision complex of O_2 and its concentration is proportional to the square of the O_2 concentration. Due to O_4 vertical profile is well known and nearly constant, it can be served as an indicator for the atmospheric distribution photon paths due to its nearly constant characteristic (Wagner et al., 2004; Frieß et al., 2006; Frieß et al., 2016). The O_4 cross-sections exhibit four main absorption bands in the UV-visible region around 360.8, 477.1, 577.1 and 630.8 nm (Thalman and Volkamer, 2013). By collecting the scattered sunlight spectra at zenith and different elevation angles closed to the horizon by MAX-DOAS, the O_4 absorptions in four bands (338-370 nm, 425-490 nm, 540-588 nm and 602-645 nm) can be estimated, and aerosol vertical profiles can be further derived (Honninger and Platt, 2002; Hytch et al., 2003; Hönninger et al., 2004; Wagner et al., 2004; Wittrock et al., 2004; Clémer et al., 2010). The sunlight at different wavelength bands has different ability to traverse the atmosphere, thus the light path length at different wavelength bands are diverse, which can change the corresponding O_4 absorptions. Conversely, the correlation analysis between O_4 absorptions retrieved at UV range and VIS range could also provide information about the impacts of aerosol scattering on photon paths (Lee et al., 2011). Besides the extinction coefficient profile and AOD, there are no detailed researches on the other AOPs retrieval based on MAX-DOAS measurements in previous. In this paper, we try to establish a new method to determine several different aerosol optical properties from multiple wavelength O_4 absorptions observed by MAX-DOAS measurement. The measurement of UV and visible O_4 absorptions was performed by MAX-DOAS instrument in Beijing from November 2016 to February 2017. Combined the O_4 absorptions and measured AOPs, some empirical relationships between them can be found under different weather conditions, which are the fundamental to determine the AOPs from MAX-DOAS observed O_4 absorptions at different wavelength bands. Furthermore, another short period measurement campaign was used to validate the feasibility and reliability of the new method to infer the AOPs under different weather conditions based on the O_4 absorptions.

2 Measurements and methodology

2.1 The MAX-DOAS measurements

The MAX-DOAS instrument was installed on the roof of the Chinese Academy of Meteorological Sciences building (CAMS, 39.9475° N, 116.3273° E) for the continuous measurements of O_4 absorptions from November 2016 to February 2017. The MAX-DOAS instrument consists of three major parts: a telescope unit, two spectrometers with temperature stabilized at 20° and a computer acting as the controlling and data acquisition unit. The viewing elevation angle of the telescope is controlled by a stepping motor. Scattered sunlight collected by the telescope is redirected by a prism reflector and a quartz fibre bundle to the spectrometers. Two spectrometers (Acton Spectrapro 300i Czerny-Turner optical spectrometer) are used to cover both the UV (300-460 nm) and visible (400-560 nm) wavelength ranges. The full-width half maximum (FWHM) spectral resolutions of these two spectrometers are all 0.6 nm, or 7.2 detector pixels. Moreover, the optical spectrometer is equipped

with a CCD detector camera (model DU 440-BU) with 2048 pixels. The field of view (FOV) of the instrument is estimated to be less than 0.5º.

A full measurement scanning sequence consists of eleven elevation angles, i.e., 1, 2, 3, 4, 5, 6, 8, 10, 15, 30 and 90°. The instrument azimuth angle is 138° and the exposure time is fixed to 60000 ms for each elevation angle measurement. A full measurement sequence takes about 11 min. Dark current and offset spectra were measured by blocking incoming light using a mechanical shutter and were subtracted from the measurement spectra before spectral analysis. The routine measurements were continuously repeated as long as the Solar Zenith Angle (SZA) was lower than 80°.

2.2 O_4 absorptions in UV and Visible

The O_4 absorptions were derived in the fitting windows of 339 to 387 nm in the UV and 425 to 490 nm in the visible spectral interval, respectively. The measured spectra were analysed using the QDOAS software developed by BIRA-IASB (http://uv-vis.aeronomie.be/software/QDOAS/). The corresponding zenith spectrum was taken as a reference spectrum for off-zenith elevation angles during each measurement scan. The DOAS fitting generates the Differential Slant Column Density (DSCD) of O_4 between the measured spectra and reference spectrum. Details of DOAS fit settings are listed in Table1. We used corrected I_0 (Aliwell et al., 2002). Figure 1 shows a typical DOAS retrieval for the O_4 absorptions at 360.8 and 477.1 nm. Afterwards, DOAS fit results with a root mean square (RMS) larger than 5×10^{-4} were filtered out, and about 99.07% of all O_4 measurements remained for the further discussion.

Table 1. DOAS retrieval settings for O_4.

Parameter	Data source	O_4 Fitting intervals	
Wavelength range		338-370 nm	425-490 nm
NO_2	298K, I_0-corrected, Vandaele et al. (1998)	√	√
NO_2	220K, I_0-corrected, Vandaele et al. (1998)	×	√
O_3	223K, I_0-corrected, Serdyuchenko et al. (2014)	√	√
O_3	243K, I_0-corrected, Serdyuchenko et al. (2014)	√	×
O_4	293K, Thalman and Volkamer (2013)	√	√
HCHO	298K, Meller and Moortgat (2000)	√	×
H2O	HITEMP (Rothman et al. 2010)	×	√
BrO	223K, Fleischmann et al. (2004)	√	×
Ring	Calculated with QDOAS	√	√
Polynomial degree		Order 5	Order 4
Intensity offset		Constant	Constant

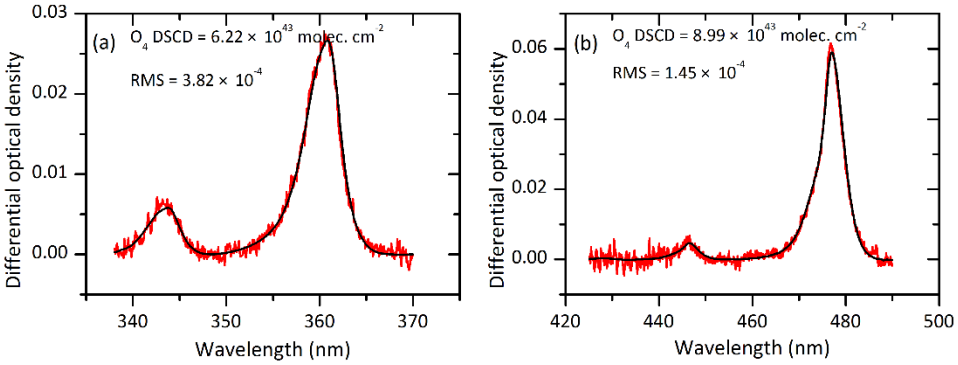

Figure 1. Typical DOAS spectral fittings for O_4 absorptions in (a) UV and (b) visible bands. Black lines represent the absorption signal and the red lines represent the sum of the absorption signal and the fit residual.

2.3 Ancillary data

Quality-assured Level 2.0 sunphotometer AODs, Asymmetric factor and Angstrom at the Beijing_CAMS AERONET site (http://aeronet.gsfc.nasa.gov/) were employed, which is collocated with the MAX-DOAS instrument just 2 meters nearby. Sunphotometer (CE-318) collects direct sunlight about every 15 minutes during non-rainy daytime. These aerosol optical parameters at multiple wavelengths were normalized to 450 nm according to Wang et al. (2016). Besides, the scattering coefficients (σ_{sca}) were measured at three wavelength (λ = 450, 520 and 700 nm) using an integrating nephelometer (Aurora 4000, Ecotech) at Peking University Urban Atmosphere Environment Monitoring Station (PKUERS, 39.9892° N, 116.3069° E).The absorption coefficients (σ_{abs}) were measured using a 7-wavelength Aethalometer (AE-31, Magee Scientific) at λ = 370, 470, 520, 660, 880 and 950 nm also located at PKUERS. Both σ_{sca} and σ_{abs} have the sampling temporal resolution of 5 minutes. In order to ensure the accuracy of the data, the corrections for σ_{sca} and σ_{abs} were referred to Shen et al. (2018). The SSA was calculated by the measured σ_{sca} at 450 nm and estimated σ_{abs} at 450 nm using the following equation:

$$SSA = \frac{\sigma_{sca}}{\sigma_{sca} + \sigma_{abs}} \quad (1)$$

The visibility and the relative humidity (RH) information were collected from the weather history data at Beijing international airport (http://www.wunderground.com/) about 26 km from CAMS. In-situ data of $PM_{2.5}$ concentrations were obtained from Guanyuan station (39.9425° N, 116.3610° E), belonging to the national environmental monitoring network (http://beijingair.sinaapp.com/data/china/sites/), which is about ~2 km from the CAMS site. All these data are normalized to hourly averages for further discussion.

3 Results

3.1 Wintertime aerosols optical properties

The time series of $PM_{2.5}$ concentrations, σ_{sca}, σ_{abs}, SSA, AOD, Angstrom, asymmetry factor and the corresponding meteorological data, i.e. RH and visibility, from November 2016 to February 2017 are presented in Fig. 2. The typical meteorological conditions of high RH and low visibility coincided with significantly high $PM_{2.5}$ concentration and high AOD. As indicated in the gray areas of Fig. 2, two episodes of particulate pollution during 15 to 22 December 2016, and 29 December 2016 to 2 January 2017 were identified.

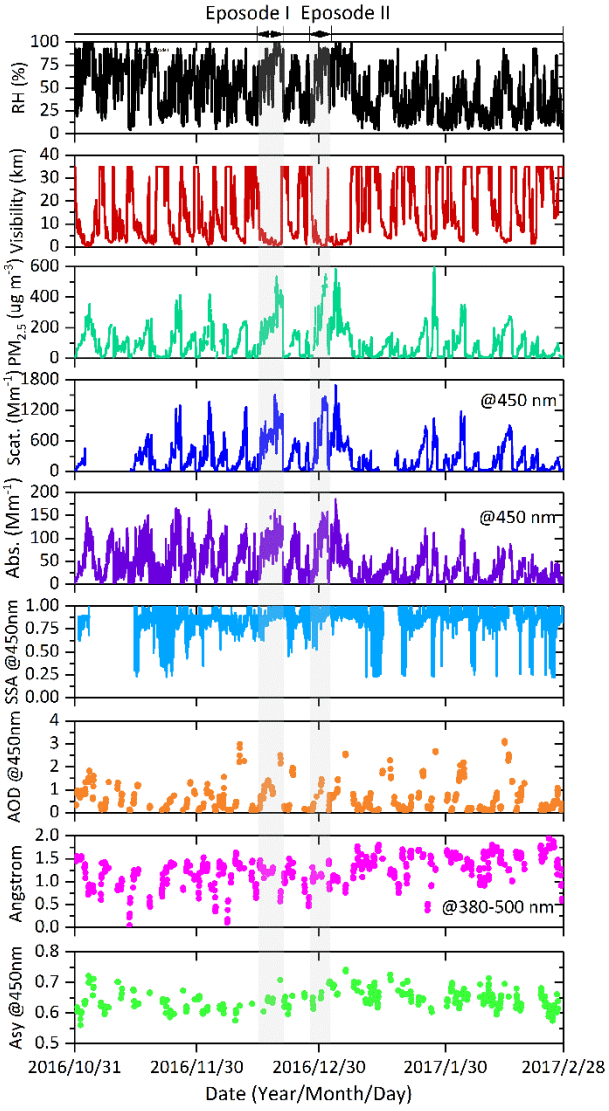

Figure 2. Time series of $PM_{2.5}$ and AOPs (σ_{sca}, σ_{abs}, SSA, AOD, Angstrom and Asymmetry factor), and meteorological parameters (relative humidity and visibility) during the observation in Beijing from November 2016 to February 2017.

During these two episodes, $PM_{2.5}$ concentrations, σ_{sca} and σ_{abs} typically increased and remained in a high level for several days, however, decrease sharply to a lower value within a shorter period. $PM_{2.5}$ concentrations, σ_{sca} and σ_{abs} increased to exceeding the maximum values 465 ug cm^{-3}, 1331.151 Mm^{-1} and 123.402 Mm^{-1} within 1-3 hours (the increment up to 200 ug cm^{-3}, 600 Mm^{-1} and 100 Mm^{-1}) during episode I, respectively. In episode II, the maximum values of $PM_{2.5}$ concentrations, σ_{sca} and σ_{abs} are 585 ug cm^{-3}, 1473.523 Mm^{-1} and 153.431 Mm^{-1}, respectively. In addition, SSA mainly kept over 0.85 during the entire wintertime, except it was observed to be less than 0.8 in late November 2016 and several days during January and February 2017. Generally, the high values of SSA were always accompanied by the peak of $PM_{2.5}$ concentrations, which suggests that the scattering properties of atmospheric aerosols were enhanced during the explosive increase stage of particles concentrations. Meanwhile, it is also associated with the decreasing of Angstrom and the increasing of asymmetry factors simultaneously. This is typically related to the particle size growth process (Guo et al., 2014; Yu et al., 2011; Yu et al., 2016).

In order to investigate the AOPs under different weather conditions, we classified observation periods of these four months into six scenarios according to the RH, visibility and $PM_{2.5}$ concentration: Clear days (Visibility > 20 km & $PM_{2.5} \leq 35$ ug m^{-3} & RH $<$ 80%), Light-haze days (10 km < Visibility $\leq$ 20 km & 35 ug m^{-3} < $PM_{2.5} \leq 75$ ug m^{-3} & RH $<$ 80%), Haze days (RH $\leq$80% & 5 km < Visibility $\leq$10 km & 75 ug m^{-3} < $PM_{2.5} \leq 115$ ug m^{-3}), Heavy-haze days (RH $\leq$ 80% & Visibility $\leq$ 5 km & $PM_{2.5}$ > 115 ug m^{-3}), Fog days (RH > 80% & Visibility $\leq$ 5 km) and Rainy days (Zheng et al., 2015; Duan et al., 2016). As expected, the AOPs showed distinct characteristics during these different weather conditions. Table 2 summarizes the statistics of Air Quality Index (AQI) and AOPs under the six scenarios. AQI is factor to comprehensively evaluate the air quality, which is based on six pollutants of ambient O_3, NO_2, CO, SO_2, PM_{10} and $PM_{2.5}$.

With the increasing of pollution level indicated by AQI (except fog and rainy days), AOD increased dramatically from 0.311 under clear days to 1.338 in heavy-haze days. There are no obvious changes for σ_{sca} and σ_{abs} between clear days and light-haze days. Nevertheless, the σ_{sca} increased sharply from light-haze days to heavy-haze days with the averaged value from 44.524 Mm^{-1} to 449.741 Mm^{-1}. The averaged value of σ_{abs} is 8.257 Mm^{-1} in light-haze days and it increased as much as 5 times in heavy-haze days. Moreover, the averaged SSA was about 0.847 on light-haze days and similar to that in haze days, but it increased about 3.53% from haze days to heavy-haze days with the averaged values from 0.846 to 0.878. It suggests that the aerosol scattering and absorption abilities have changed evidently but the ratio of scattering to extinction have changed slightly during the processes of particle pollution became severe. No obvious variations on Angstrom were observed among clear days to heavy-haze days, but it decreased by about 2.83% in fog days. In previous study, the Angstrom are usually higher than 0.80 when AOD is greater than 0.60 in Beijing, which reveals the major contribution of small particles for higher aerosol loading (Che et al., 2015). However, our study demonstrates that small particles made a major contribution to the aerosols throughout the whole wintertime in Beijing. The obvious decrease of Angstrom in fog days is attributed to the increase of

water vapour in particles. In addition, the averaged asymmetry factor was about 0.697 in fog days and 8.52% higher than other weather conditions. It indicates the increased forward scattering in fog days (Yoon and Kim, 2006).

Table 2. Statistics of AQI and several aerosol optical properties under different weather conditions.

Weather condition / AQI and AOPs	Clear day: Visibility > 20 km & $PM_{2.5} \leq 35$ ug m^{-3} & RH < 80%			Light-haze day: 10 km < Visibility ≤ 20 km & 35 ug m^{-3} < $PM_{2.5} \leq 75$ ug m^{-3} & RH < 80%			Haze day: 5 km < Visibility ≤ 10 km & 75 ug m^{-3} < $PM_{2.5} \leq 115$ ug m^{-3} & RH < 80%			Heavy-haze day: Visibility ≤ 5 km & $PM_{2.5}$ > 115 ug m^{-3} & RH < 80%			Fog day: Visibility ≤ 5 km & RH > 80%			Rainy day: RH > 80%		
	Ave.	min	max	Ave.	min	max	Ave.	min	max	Ave.	min	max	Ave.	min	max	Ave.	min	max
AQI	24	5	44	60	15	119	130	39	391	214	43	500	306	26	500	106	15	500
σ_{abs}	7.356	0.605	63.999	8.257	1.003	37.229	39.985	2.142	103.421	53.257	3.322	105.290	89.625	7.634	156.878	28.137	2.296	94.639
σ_{sca}	41.411	3.920	214.581	44.524	8.889	305.853	259.081	5.872	809.550	449.741	14.093	1096.859	739.152	53.895	1662.896	217.125	25.938	656.143
SSA	0.854	0.419	0.975	0.847	0.518	0.953	0.846	0.438	0.931	0.878	0.686	0.930	0.887	0.790	0.928	0.878	0.764	0.941
Asy	0.640	0.560	0.714	0.643	0.599	0.670	0.639	0.575	0.704	0.647	0.598	0.742	0.697	0.660	0.708			
Angstrom	1.252	0.210	1.943	1.304	0.429	1.950	1.265	0.176	1.853	1.286	0.798	1.731	1.054	0.568	1.759			
AOD	0.311	0.051	0.799	0.351	0.103	0.927	0.892	0.645	2.495	1.338	0.939	2.693	0.998	0.105	2.509			

3.2 UV and visible O_4 absorptions under different weather conditions

Figure. 3 shows the examples of diurnal pattern and corresponding correlation of UV and visible O_4 DSCDs (elevation angle = 1°) at 360.8 and 477.1 nm under five different weather conditions, except for the rainy days. In view of the absolute strength of O_4 absorption, both the O_4 DSCDs in the UV and visible bands varied in the order of clear days > light-haze days > haze days > heavy-haze days > fog days. It manifested the dependency of O_4 absorption on the scattering sunlight path impacted by the aerosol loading. Moreover, O_4 DSCDs at 477.1 nm are obviously higher than that at 360.8 nm in clear and light-haze days, and slightly larger than that at 360.8 nm in haze and heavy-haze days, which can be explained by the fact that the observable light path length at visible range is longer than UV range. Even in UV bands, the observed O_4 DSCDs at 353 nm were reported to be lower than those at 380 nm for most of the elevations under haze conditions during winter in Beijing (Lee et al. 2011). This phenomenon revealed that O_4 absorptions in short wavelength range were more significantly affected by light diffusion under hazy conditions. However, we found there is no obvious differences between O_4 DSCDs at 360.8 and 477.1 nm in fog days, during which the high contents of water vapour decreased the visibility and the atmospheric absorption paths from UV to visible range.

We further analysed the relationship of O_4 absorptions between UV and visible bands. As shown in the right column of Fig. 3, the correlation coefficient (R^2) of O_4 DSCDs between at 360.8 and 477.1 nm varied in the order of clear days > light-haze days > haze days > heavy-haze days. Strong correlation between UV and visible O_4 absorptions ($R^2 > 0.9$) was achieved for clear and light-haze days. Under haze and heavy-haze conditions, R^2 was 0.81 and 0.74, respectively, which are much lower than that in clear and light-haze days. That is because the increase of light-absorbing and light-scattering aerosols can result in reduced light path lengths more obviously in shorter wavelength bands than longer wavelength bands during haze and heavy-haze days.

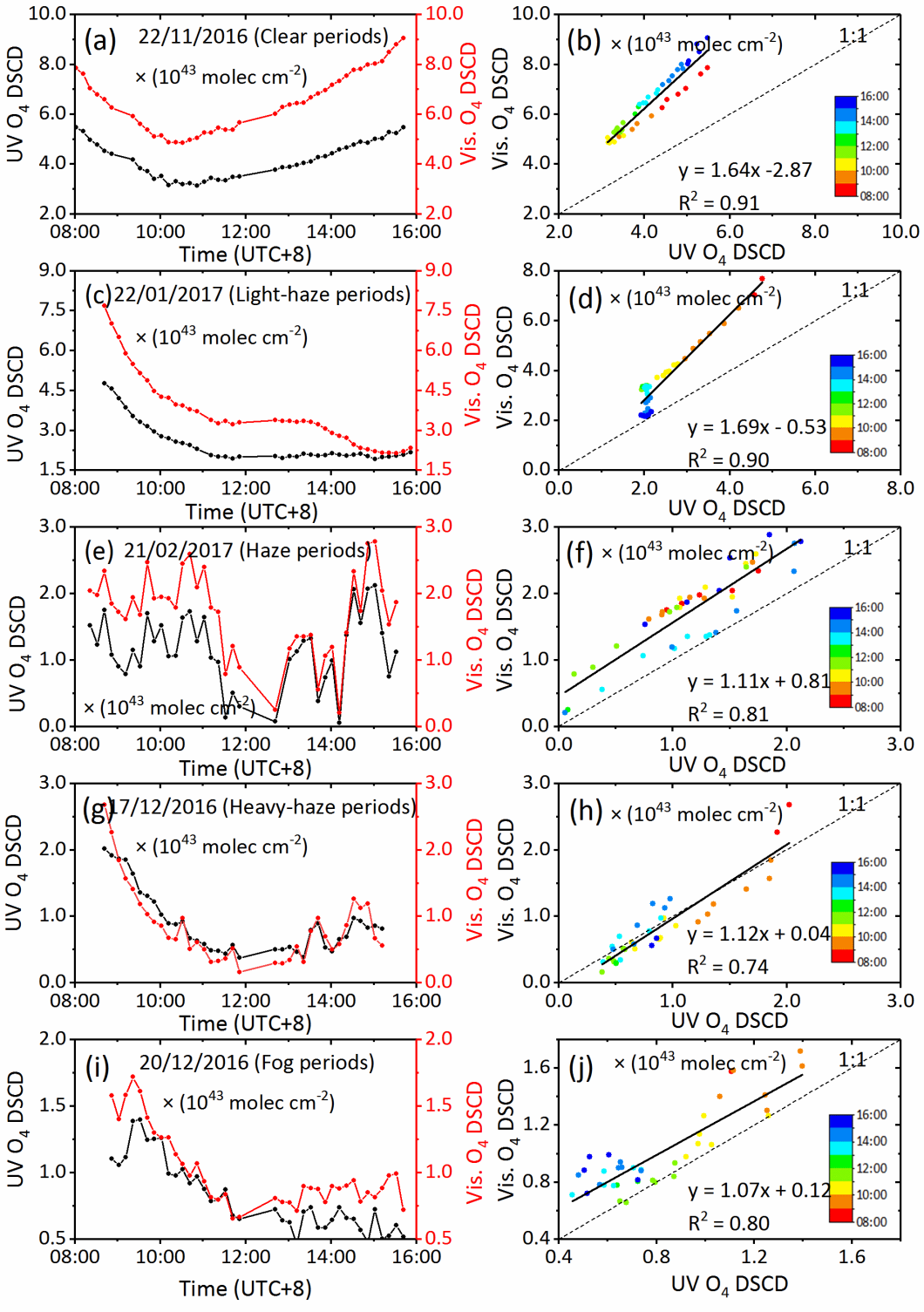
(a) 22/11/2016 (Clear periods)
× (10^43 molec cm^-2)
UV O4 DSCD
Vis. O4 DSCD
Time (UTC+8)
(b) × (10^43 molec cm^-2)
1:1
y = 1.64x -2.87
R^2 = 0.91
(c) 22/01/2017 (Light-haze periods)
(d) y = 1.69x - 0.53
R^2 = 0.90
(e) 21/02/2017 (Haze periods)
(f) y = 1.11x + 0.81
R^2 = 0.81
(g) 17/12/2016 (Heavy-haze periods)
(h) y = 1.12x + 0.04
R^2 = 0.74
(i) 20/12/2016 (Fog periods)
(j) y = 1.07x + 0.12
R^2 = 0.80
16:00
14:00
12:00
10:00
08:00

Figure 3. Diurnal variation and correlation analysis of O_4 DSCDs at 360.8 and 477.1 nm under different weather conditions: (a) and (b) clear day, (c) and (d) light-haze day, (e) and (f) haze day, (g) and (h) heavy-haze day, (i) and (j) fog day. The colorbar represents the time sequence.

The changes of AOPs, especially aerosol scattering and absorption properties, are mainly manifested in the variations of O_4 absorptions at different wavelength bands. The correlation information of O_4 DSCDs at different bands will also be affected by the variation of AOPs. For more detailed, i.e., 21 February 2017, was chosen to exhibit the influence of AOPs changes on O_4 DSCDs in Fig. 4. Compared Fig. 4 (a) to (b), it can be found that σ_{sca} and σ_{abs} have a similar variation trends, a slightly turning and an abruptly decrease occurred at ~09:05 and ~12:00 (especially for σ_{sca}), respectively, while the time-indicated O_4 DSCDs seems to be three segments with higher correlation coefficient divided by the break point of 10:00 and 12:00.

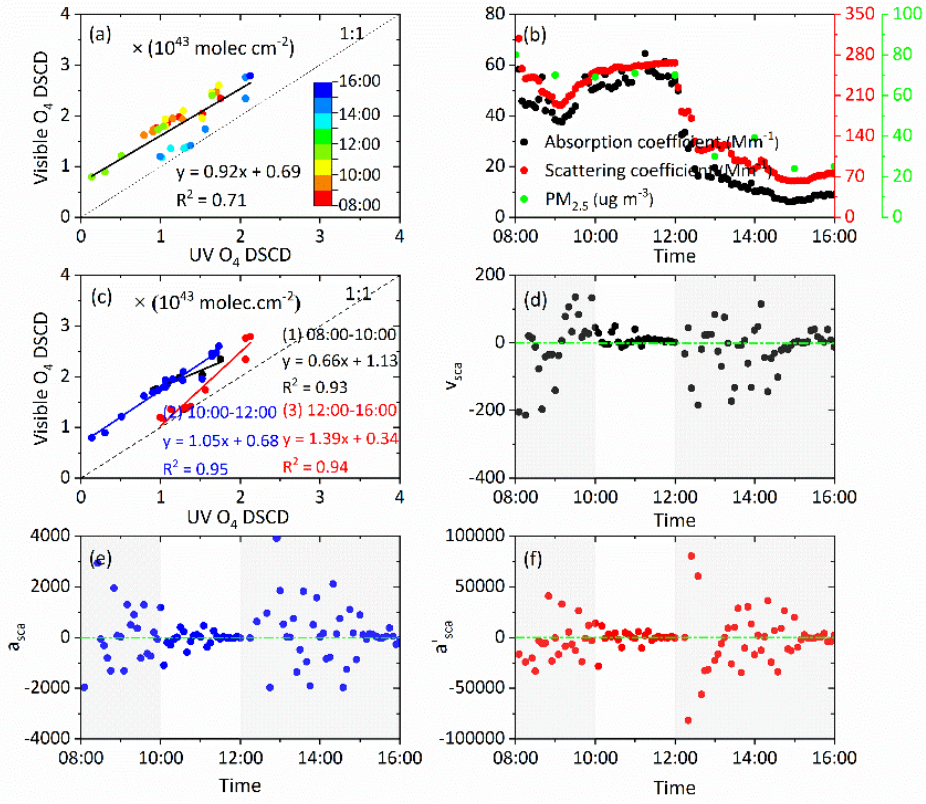

Figure 4. An example day on 21 February 2017: (a) the correlations between O_4 DSCDs at 360.8 and 477.1 nm. The colorbar represents time sequence. (b) shows the time series of aerosol scattering and absorption coefficients. The correlations information between O_4 DSCDs at 360.8 and 477.1 nm on 08:00-10:00, 10:00-12:00 and 12:00-16:00 21 February 2017 were shown in (c). (d) to (f) shows the time series of v_{sca}, a_{sca} and a'_{sca} of scattering coefficients, respectively.

In order to explore the relationship between the O_4 DSCDs at different wavelength bands and the variations of σ_{sca} and σ_{abs}, we defined the change speed (v_{sca}), acceleration (a_{sca}) and the change rate of acceleration (a'_{sca}) of σ_{sca} (Fig4 (b), (e) and (f)) as the following three equations,

$$v_{sca} = \frac{d_{sca}}{dt} \quad (2)$$

$$a_{sca} = \frac{d_{v_{sca}}}{dt} \quad (3)$$

$$a'_{sca} = \frac{d_{a_{sca}}}{dt} \quad (4)$$

Accordingly, the relevant time series of v_{sca}, a_{sca} and a'_{sca} are displayed in Fig. 4 (d) to (f). In this case, we can find two time break points, defined as t_1 and t_2 (t_1 = 10:00 and t_2 = 12:00), at which σ_{sca} and σ_{abs} have significant variations based on the calculated v_{sca}, a_{sca} and a'_{sca}. In addition, we found the indicator of a'_{sca} can describe the specific moment at which the change (increasing or decreasing) of σ_{sca} more clearly than v_{sca} and a_{sca} in this case. $|a'_{scat_1}|$ and $|a'_{scat_2}|$ are all higher than 20000. Consequently, the O_4 DSCDs at 360.8 and 477.1 nm can be divided into three segments for the periods of 08:00-10:00, 10:00-12:00 and 12:00-16:00 and the correlation between UV and VIS O_4 DSCDs was further analysed individually. As shown in Fig. 4(c), the R^2 during 08:00-10:00 and 10:00-12:00 is obviously larger than that of all day in Fig. 4(a), however, it is smaller for segment of 12:00-16:00. Moreover, there were huge divergences among the correlation slopes among these three segments due to the change of aerosol scattering and absorption properties. Therefore, it can be concluded that the diurnal variations of O_4 DSCDs provide the information of the light path length impacted by aerosol loading, and further the varied relationship between O_4 DSCDs at UV and visible implies the change of the aerosol scattering and absorption properties.

Using the method discussed above, we have defined the time break points with aerosol properties changes and further classified the observation into several segmental periods with the criterion of $|v_{sca}| > 1000$ or $|a_{sca}| > 10000$ or $|a'_{sca}| > 20000$. The summary of time break points and corresponding change speed (v_{sca}), acceleration (a_{sca}) and the change rate of acceleration (a'_{sca}) of σ_{sca} were listed in Table S1.

3. 3 Implications of O_4 absorptions to aerosol optical properties

In order to derive the aerosol optical properties from multiple wavelength O_4 absorptions, the complete four months observational O_4 and AOPs data were used for discussion under different weather conditions. Hourly data of O_4 DSCDs were divided into five weather conditions and made the linear regression between UV and VIS O_4 DSCDs. In total, there were about 218 segments (776 hours in 97 days), including 67, 31, 61, 44 and 15 segments for clear, light-haze, haze, heavy-haze and fog days, respectively. Figure 5 illustrated the statistics of O_4 DSCDs in UV and visible bands, and the slope and R^2 of correlation analysis between them, as well as the O_4 DSCDs ratio of UV to visible for different weather conditions.

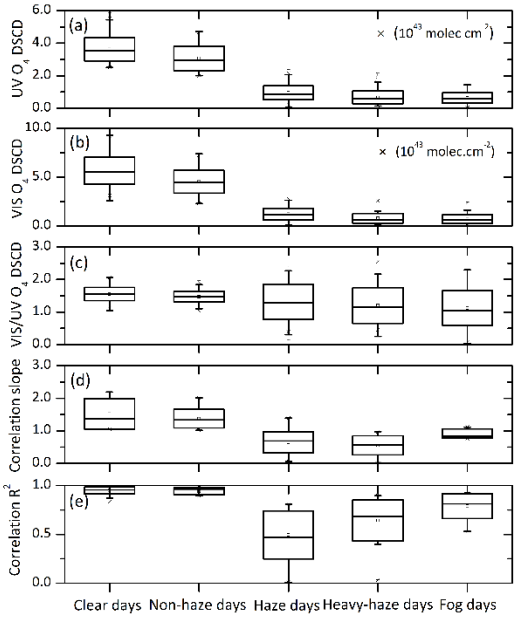

Figure 5. Box plots of statistics for the O_4 DSCD under different weather conditions: (a) in the UV band, (b) in the visible band, (c) the ratio of VIS/UV O_4 DSCD, (d) correlation slope and (e) R^2 between UV and visible (Visible O_4 DSCD=slope*UV O_4 DSCD + intercept).

In general, the O_4 DSCDs in UV are mainly ranged in 3.00-4.00 × 10^{43}, 2.50-3.50 × 10^{43}, 0.50-1.10 × 10^{43}, 0.25-0.80 × 10^{43} and 0.20-0.40 × 10^{43} molec cm^{-2} in clear, light-haze, haze, heavy-haze and fog days, respectively. And the O_4 DSCDs in visible are mainly distributed between 4.00-6.50 × 10^{43}, 3.00-5.50 × 10^{43}, 0.50-1.30 × 10^{43}, 0.25-0.60 × 10^{43} and 0.25-0.60 × 10^{43} molec cm^{-2} under above five different weather conditions, which are higher than those in UV especially for clear and light-haze days. Moreover, the corresponding ratio of visible to UV O_4 DSCDs are 1.45-1.70, 1.45-1.65, 1.00-1.65, 0.85-1.35 and 0.80-1.35 under these five weather conditions, respectively. The linear regression results show that the correlation slopes between UV and visible O_4 DSCDs are greater than 1.00 (mainly greater than 1.40) and the correlation R^2 are greater than 0.93 mostly in clear days. Under light-haze condition, the correlation slopes are greater than 1.00 (mainly greater than 1.20) and the correlation R^2 are mainly greater than 0.90, respectively. The correlation slopes are mainly less than 0.60 and the correlation R^2 have a wider range (the maximum value < 0.80 and occasional fitting failure) in haze days. In heavy-haze days, the correlation slopes are less than 0.60-0.80 and the correlation R^2 are 0.50-0.80 mostly (some fitting failure cases appeared). In fog days, the correlation slopes are floated around 1.00 and the correlation R^2 are mainly 0.75-0.85, respectively.

Meanwhile, the statistical characteristics of AOPs under different weather conditions are shown in Fig. 6. Similar to the results in Table 2, σ_{sca} shows the increasing trend and were mainly distributed between 21.83-47.01, 28.33-57.25, 134.72-349.47, 228.42-649.11 and 450.00-1004.88Mm^{-1} in clear, light-haze, haze, heavy-haze and fog days, respectively. The σ_{abs} were mainly distributed between 2.61-8.26, 3.99-11.89, 22.25-57.31, 34.84-72.22 and 70.01-115.26 Mm^{-1} under above five different

weather conditions. The AODs were mainly distributed between 0.11-0.35, 0.12-0.37, 0.76-1.70, 1.37-2.38 and 0.69-1.38 under these five weather conditions. The Angstrom were more disperse for clear and light-haze days than the other weather conditions. Except the fog days, the asymmetry factor in other weather conditions are not much different.

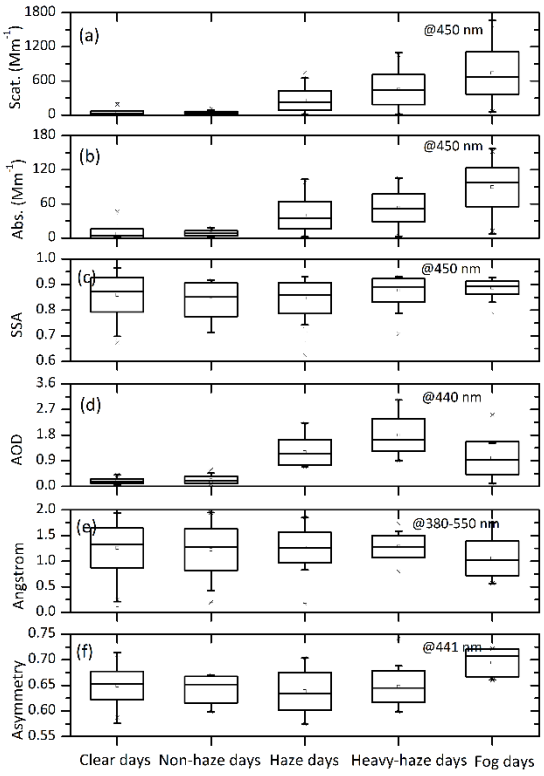

Figure 6. Box plots of the statistics on aerosol optical properties under different weather conditions: (a) σ_{sca}, (b) σ_{abs}, (c) SSA, (d) AOD, (e) Angstrom and (f) Asymmetry.

Combined the statistical information on O_4 absorptions and AOPs, we could conclude some empirical relationships as following:

(1) Under the condition that the correlation slopes between UV and visible O_4 DSCDs greater than 1.0 and the correlation R^2 greater than 0.9, simultaneously, the UV and visible O_4 DSCDs are mainly greater than 2.5×10^{43} molec cm^{-2} and 3.0×10^{43} molec cm^{-2}, we could know the weather mainly should be clear or light-haze days. It can be suspected that σ_{sca} and σ_{abs} are less than 45 Mm^{-1} and 12 Mm^{-1}, and AODs are less than 0.4.

(2) Under the condition of the correlation slope less than 0.6 and the correlation R^2 less than 0.8, simultaneously, the UV and visible O_4 DSCDs are mainly less than 1.1×10^{43} molec cm^{-2} and 1.3×10^{43} molec cm^{-2}, the weather mainly should be haze or heavy-haze days. Moreover, σ_{sca} and σ_{abs} are estimated to be distributed at 200-900 Mm^{-1} and 20-60 Mm^{-1},

respectively. AODs are between 0.9 and 2.5. In more detail, σ_{sca}, σ_{abs} and AOD will be located at 200-400 Mm^{-1}, 20-50 Mm^{-1} and 0.9-1.5 under the condition of UV and visible O_4 DSCDs > 1.0×10^{43} molec.cm^{-2}.

(3) If the correlation slope floating around 1.0 and with a correlation R^2 of 0.75-0.85, we could know the weather mainly should be fog days. σ_{sca} and σ_{abs} are located at 450-1200 $Mm^{-1}$and 60-90 Mm^{-1}, while AODs are greater than 0.7.

Therefore, it represents the potential ability to determine the basic aerosol loading conditions from the MAX-DOAS observed O_4 absorptions.

4 Discussion

To investigate the feasibility and reliability, another short period MAX-DOAS measurement campaign operated in Gucheng, Hebei province (39.1382° N, 115.7163° E) from 19 to 27 November 2016 was used for the application of the new method to determine AOPs from O_4 absorptions. The MAX-DOAS instrument is the same as that one installed in CAMS. Due to absence of sunphotometer instrument, AODs at 450 nm were obtained by profiling the aerosol extinction coefficient based on MAX-DOAS measurements by utilizing the optimal estimation method (Frieß et al., 2006; Frieß et al., 2016; Xing et al., 2017). Besides, σ_{sca} and σ_{abs} were acquired using the co-located same integrating nephelometer (Aurora 1000, Ecotech) and 7-wavelength Aethalometer (AE-31, Magee Scientific), respectively. Moreover, the temporal resolution of σ_{sca} and σ_{abs} measurements are 1 minute and 1 hour, respectively.

Figure 7(a) and (b) shows the diurnal variations and segmental correlation of O_4 DSCDs in UV and visible bands during this campaign. According to the empirical relationships discussed in section 3.3, it can be inferred that the period segment during 09:00-11:00 in 25 November should be haze or heavy-haze condition, because the UV and VIS O_4 DSCDs are all less than 0.5×10^{43} molec cm^{-2}, and simultaneously the correlation slope and R^2 between them are 0.42 and 0.59, which are in line with the determination conditions that UV and visible O_4 DSCDs are mainly less than 1.1×10^{43} and 1.3×10^{43} molec cm^{-2}, simultaneously combined the correlation slope and R^2 between them are mainly less than 0.6 and 0.8. Similarly, other periods that 09:00-12:00 of 21 Nov., 10:50-16:00 of 22 Nov., 10:00-15:00 of 23 Nov., 08:00-15:00 of 26 Nov. and 11:00-15:00 of 27 Nov. are mainly clear or light-haze weather type. And 09:00-10:00 of 19 Nov., 09:00-12:00 of 20 Nov. and 09:00-10:50 of 22 Nov. can be mainly regarded as haze or heavy-haze weather types.

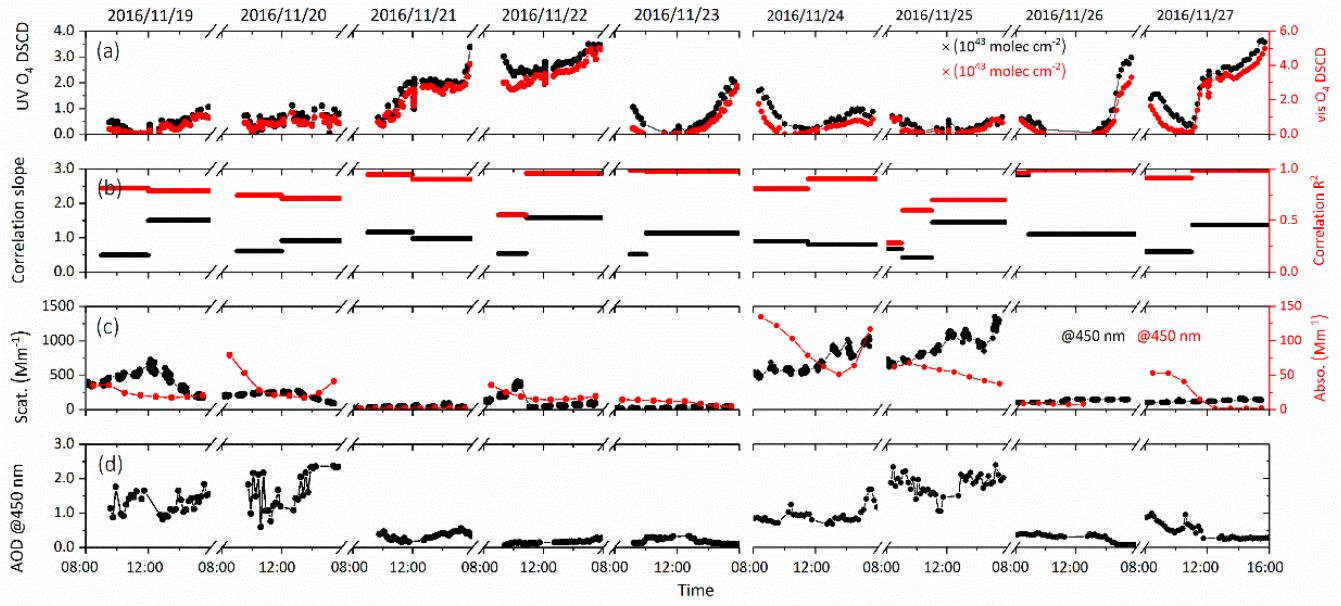

Figure 7. Time series of O_4 absorptions and aerosol optical properties at Gucheng, Hebei from 19 to 27 November 2016: (a) UV and visible O_4 DSCDs, (b) correlation slopes and R^2 between O_4 DSCDs at 360.8 and 477.1 nm, (c) σ_{sca} and σ_{abs} at 450 nm, (d) AOD at 450 nm retrieved by MAX-DOAS.

Furthermore, the time series of in-situ σ_{sca}, σ_{abs} and MAX-DOAS retrieved AOD are shown in Fig.7 (c) and (d). According to the empirical relationships summarized above, the σ_{sca}, σ_{abs} and AOD are mainly located at 200-900 Mm^{-1}, 20-60 Mm^{-1} and 0.9-2.5 under the haze segment of 09:00-11:00 of 25 November. Simultaneously, the in-situ measured σ_{sca}, σ_{abs} and MAX-DOAS retrieved AOD during the above same periods are ranged in 588.30-730.77 Mm^{-1}, 58.19-67.63 Mm^{-1} and 1.39-2.22. The inferred results are in good agreement with the measured results. It indicates that the concluded empirical relationships can be used as the criterion to accurately determine the ranges of aerosol optical parameters of σ_{sca}, σ_{abs} and AOD. Nevertheless, we found two segments with correlation slopes > 1.0 and R^2 < 0.9 during 12:00-15:00 of 19 Nov. and 11:00-15:00 of 25 Nov., which is not included in cases of the empirical relationships. It suggests that more refined and quantitative relationships between aerosol optical parameters and O_4 absorptions need to be further achieved with the increases of the measured data, which can be established as a look up table to retrieve the aerosol optical properties in the future.

Moreover, in order to illustrate the variations on the O_4 absorptions due to the change of aerosol loadings, we used radiative transfer model of SCIATRAN to simulate O_4 DSCDs in UV and Visible bands under conditions with different aerosol optical properties. In total, 11 different aerosol scenarios were simulated and further the linear-regression analysis for the simulated UV and Visible O_4 DSCDs under different aerosol conditions were performed. The forward RTM simulation results presented in the Supplement (Table S2 and Figure S1) demonstrate that the O_4 absorptions information, including the value of UV and

Visible O_4 DSCDs, the corresponding linear-regression slope and R^2 between them, could greatly reflect the variation of aerosol optical properties. More details can be referred in the Supplement.

5 Summary and conclusions

Ground-based MAX-DOAS measurements for O_4 DSCDs in the UV and visible wavelength bands were carried out in Beijing from November 2016 to February 2017. Combined with the measured σ_{sca} and σ_{abs} and AOD, we have summarized the characteristics of O_4 absorptions and parameters of AOPs under different weather conditions during autumn-winter seasons. It was found that the averaged AOD increased from 0.311 in clear days to 1.338 in heavy-haze days. The averaged σ_{sca} changed dramatically from 44.524 Mm^{-1} in light-haze days to 449.741 Mm^{-1} in heavy-haze days. Moreover, the averaged σ_{abs} also obviously increased from 8.257 Mm^{-1} in light-haze days to 53.257 Mm^{-1} of heavy-haze condition. Both the measured UV and visible O_4 DSCDs varied in the order of clear days > light-haze days > haze days > heavy-haze days > fog days. The corresponding correlation information (slope and R^2) between O_4 DSCDs at UV and visible wavelength bands also changed synchronously when σ_{sca} and σ_{abs} have varied.

Considering the simultaneous variation of O_4 absorptions and AOPs, the segmental periods correlations analysis between UV and visible O_4 DSCDs were performed. Afterwards, the empirical relationships between O_4 absorptions and AOPs can be concluded for different aerosol loadings. It could be clear and light-haze days under the condition of linear-regression slopes are greater than 1.0 and R^2 mainly greater than 0.9, simultaneously, UV and Visible O_4 DSCDs are mainly greater than 2.5×10^{43} molec cm^{-2}. σ_{sca}, σ_{abs} and AOD are mainly less than 45 Mm^{-1}, 12 Mm^{-1} and 0.4 under this condition, respectively. When the correlation slopes, R^2 and O_4 DSCDs are less than 0.6, 0.8 and 1.3×10^{43} molec cm^{-2}, respectively, it mainly should be haze or heavy-haze days. Under this condition, the σ_{sca}, σ_{abs} and AOD can be inferred to be mainly located at 200-900 Mm^{-1}, 20-60 Mm^{-1} and 0.9-2.5, respectively. In addition, it should be fog days if the correlation slopes float around 1.0 and R^2 of 0.75-0.85. Another MAX-DOAS measurement campaign carried out at Gucheng from 19 to 27 November 2016 were used to validate the proposed new method, which could well determine the AOPs from the observed O_4 absorptions.

In this paper, we present a new method to deduce directly the parameters of aerosol optical properties from the observed UV and visible O_4 absorptions, which expands the usages of MAX-DOAS technique to fast semi-quantify the aerosol scattering and absorption properties. With the improvement of the look-up table, more precise and accurate inversion of aerosol optical properties can be achieved. Since only the O_4 DSCDs at elevation angle of 1° were employed to obtain the aerosol scattering and absorption at surface, it can be expected that vertical spatial-resolved of aerosol scattering and absorption can be retrieved by using O_4 DSCDs at different elevation angles in the future study.

Acknowledgements

This research was supported by grants from National Key Research and Development Program of China (2018YFC0213104, 2018YFC0213100, 2016YFC0203302, 2017YFC0210002), National Natural Science Foundation of China (41722501, 91544212, 51778596, 41575021), and Shanghai Pujiang Talent Program (17PJC015). We would like to thank CAMS and Peking University for the data of σ_{sca} and σ_{abs} measured in Gucheng and PKUERS, respectively.

References

Allen, R. J., Sherwood, S. C., Norris, J. R., and Zender, C. S.: Recent Northern Hemisphere tropical expansion primarily driven by black carbon and tropospheric ozone, Nature, 485, 350-354, doi:10.1038/nature11097, 2012.

Bergstrom, R. W., Pilewskie, P., Russell, P. B., Redemann, J., Bond, T. C., Quinn, P. K., and Sierau, B.: Spectral absorption properties of atmospheric aerosols, Atmospheric Chemistry and Physics, 7, 5937-5943, 2007.

Che, H., Xia, X., Zhu, J., Wang, H., Wang, Y., Sun, J., Zhang, X., and Shi, G.: Aerosol optical properties under the condition of heavy haze over an urban site of Beijing, China, Environmental science and pollution research international, 22, 1043-1053, doi:10.1007/s11356-014-3415-5, 2015.

Clémer, K., Van Roozendael, M., Fayt, C., Hendrick, F., Hermans, C., Pinardi, G., Spurr, R., Wang, P., and De Mazière, M.: Multiple wavelength retrieval of tropospheric aerosol optical properties from MAX-DOAS measurements in Beijing, Atmospheric Measurement Techniques, 3, 863-878, 10.5194/amt-3-863-2010, 2010.

Ding, A. J., Huang, X., Nie, W., Sun, J. N., Kerminen, V. M., Petäjä, T., Su, H., Cheng, Y. F., Yang, X. Q., Wang, M. H., Chi, X. G., Wang, J. P., Virkkula, A., Guo, W. D., Yuan, J., Wang, S. Y., Zhang, R. J., Wu, Y. F., Song, Y., Zhu, T., Zilitinkevich, S., Kulmala, M., and Fu, C. B.: Enhanced haze pollution by black carbon in megacities in China, Geophysical Research Letters, 43, 2873-2879, doi:10.1002/2016gl067745, 2016.

Duan, L., Xiu, G., Feng, L., Cheng, N., and Wang, C.: The mercury species and their association with carbonaceous compositions, bromine and iodine in $PM_{2.5}$ in Shanghai, Chemosphere, 146, 263-271, 10.1016/j.chemosphere.2015.11.058, 2016.

Dubovik, O., Holben, B. R., Eck, T. F., Smirnov, A., Kaufman, Y. J., King, M. D., Tanre, D., and Slutsker, I.: Variability of Absorption and Optical Properties of Key Aerosol Types Observed in Worldwide Locations, Journal of the Atmospheric Sciences, 59, 590-607, 2001.

Eck, T. F., Holben, B. N., Reid, J. S., O'Neill, N. T., Schafer, J. S., Dubovik, O., Smirnov, A., Yamasoe, M. A., and Artaxo, P.: High aerosol optical depth biomass burning events: A comparison of optical properties for different source regions, Geophysical Research Letters, 30, NO. 20, 2035, doi:10.1029/2003gl017861, 2003.

Eck, T. F., Holben, B. N., Dubovik, O., Smirnov, A., Goloub, P., Chen, H. B., Chatenet, B., Gomes, L., Zhang, X. Y., Tsay, S. C., Ji, Q., Giles, D., and Slutsker, I.: Columnar aerosol optical properties at AERONET sites in central eastern Asia and

aerosol transport to the tropical mid-Pacific, Journal of Geophysical Research: Atmospheres, 110, D06202, doi:10.1029/2004jd005274, 2005.

Frieß, U., Monks, P. S., Remedios, J. J., Rozanov, A., Sinreich, R., Wagner, T., and Platt, U.: MAX-DOAS O4measurements: A new technique to derive information on atmospheric aerosols: 2. Modeling studies, Journal of Geophysical Research, 111, doi:10.1029/2005jd006618, 2006.

Frieß, U., Klein Baltink, H., Beirle, S., Clémer, K., Hendrick, F., Henzing, B., Irie, H., de Leeuw, G., Li, A., Moerman, M. M., van Roozendael, M., Shaiganfar, R., Wagner, T., Wang, Y., Xie, P., Yilmaz, S., and Zieger, P.: Intercomparison of aerosol extinction profiles retrieved from MAX-DOAS measurements, Atmospheric Measurement Techniques, 9, 3205-3222, doi:10.5194/amt-9-3205-2016, 2016.

Fyfe, J. C., Gillett, N. P., and Zwiers, F. W.: Overestimated global warming over the past 20 years, Nature Climate Change, 3, 767-769, 10.1038/nclimate1972, 2013.

Galdos, M., Cavalett, O., Seabra, J. E. A., Nogueira, L. A. H., and Bonomi, A.: Trends in global warming and human health impacts related to Brazilian sugarcane ethanol production considering black carbon emissions, Applied Energy, 104, 576-582, 10.1016/j.apenergy.2012.11.002, 2013.

Garland, R. M., Schmid, O., Nowak, A., Achtert, P., Wiedensohler, A., Gunthe, S. S., Takegawa, N., Kita, K., Kondo, Y., Hu, M., Shao, M., Zeng, L. M., Zhu, T., Andreae, M. O., and Pöschl, U.: Aerosol optical properties observed during Campaign of Air Quality Research in Beijing 2006 (CAREBeijing-2006): Characteristic differences between the inflow and outflow of Beijing city air, Journal of Geophysical Research, 114, doi:10.1029/2008jd010780, 2009.

Guo, L., Guo, X., Fang, C., and Zhu, S.: Observation analysis on characteristics of formation, evolution and transition of a long-lasting severe fog and haze episode in North China, Science China Earth Sciences, 58, 329-344, doi:10.1007/s11430-014-4924-2, 2014.

Hönninger, G., Friedeburg, C. v., and Platt, U.: Multi axis differential optical absorption spectroscopy (MAX-DOAS), Atmospheric Chemistry and Physics, 4, 231-254, 2004.

He, X., L, C. C., Lau, A. K. H., Deng, Z. Z., Mao, J. T., Wang, M. H., and Liu, X. Y.: An intensive study of aerosol optical propertiesin Beijing urban area, Atmospheric Chemistry and Physics, 9, 8903-8915, 2009.

Hess, M., Koepke, P., and Schult, I.: Optical Properties of Aerosols and Clouds: The Software Package OPAC Bull. Amer. Meteor. Soc., 79, 831-844, 1998.

Honninger, G., and Platt, U.: Observations of BrO and its vertical distribution during surface ozone depletion at Alert, Atmospheric Environment, 36, 2481-2489, 2002.

Huang, R. J., Zhang, Y., Bozzetti, C., Ho, K. F., Cao, J. J., Han, Y., Daellenbach, K. R., Slowik, J. G., Platt, S. M., Canonaco, F., Zotter, P., Wolf, R., Pieber, S. M., Bruns, E. A., Crippa, M., Ciarelli, G., Piazzalunga, A., Schwikowski, M., Abbaszade, G., Schnelle-Kreis, J., Zimmermann, R., An, Z., Szidat, S., Baltensperger, U., El Haddad, I., and Prevot, A. S.: High secondary aerosol contribution to particulate pollution during haze events in China, Nature, 514, 218-222, 10.1038/nature13774, 2014.

Hytch, M. J., Putaux, J. L., and Penisson, J. M.: Measurement of the displacement field of dislocations to 0.03 A by electron microscopy, Nature, 423, 270-273, doi:10.1038/nature01638, 2003.

Karanasiou, A., Moreno, N., Moreno, T., Viana, M., de Leeuw, F., and Querol, X.: Health effects from Sahara dust episodes in Europe: literature review and research gaps, Environment international, 47, 107-114, 10.1016/j.envint.2012.06.012, 2012.

Kaufman, Y. J., Tanré, D., Dubovik, O., Karnieli, A., and Remer, L. A.: Absorption of sunlight by dust as inferred from satellite and ground-based remote sensing, Geophysical Research Letters, 28, 1479-1482, doi:10.1029/2000gl012647, 2001.

Kim, D., and Ramanathan, V.: Solar radiation budget and radiative forcing due to aerosols and clouds, Journal of Geophysical Research, 113, doi:10.1029/2007jd008434, 2008.

Lee, H., Irie, H., Gu, M., Kim, J., and Hwang, J.: Remote sensing of tropospheric aerosol using UV MAX-DOAS during hazy conditions in winter: Utilization of O4 Absorption bands at wavelength intervals of 338–368 and 367–393 nm, Atmospheric Environment, 45, 5760-5769, 10.1016/j.atmosenv.2011.07.019, 2011.

Levy, H., Horowitz, L. W., Schwarzkopf, M. D., Ming, Y., Golaz, J.-C., Naik, V., and Ramaswamy, V.: The roles of aerosol direct and indirect effects in past and future climate change, Journal of Geophysical Research: Atmospheres, 118, 4521-4532, doi:10.1002/jgrd.50192, 2013.

Liousse, C., Penner, J. E., Chuang, C., Walton, J. J., Eddleman, H., and Cachier, H.: A global three-dimensional model study of carbonaceous aerosols, in: Journal of Geophysical Research: Atmospheres, D14, 19411-19432, 1996.

Platt, U., and Stutz, J.: Differential Optical Absorption Spectroscopy, 3, 540-75776, 2008.

Ramana, M. V., Ramanathan, V., Feng, Y., Yoon, S. C., Kim, S. W., Carmichael, G. R., and Schauer, J. J.: Warming influenced by the ratio of black carbon to sulphate and the black-carbon source, Nature Geoscience, 3, 542-545, 10.1038/ngeo918, 2010.

Ramanathan, V., Ramana, M. V., Roberts, G., Kim, D., Corrigan, C., Chung, C., and Winker, D.: Warming trends in Asia amplified by brown cloud solar absorption, Nature, 448, 575-578, doi:10.1038/nature06019, 2007.

Remer, L. A., and Kaufman, Y. J.: Dynamic aerosol model: Urban/industrial aerosol, Journal of Geophysical Research: Atmospheres, 103, 13859-13871, doi:10.1029/98jd00994, 1998.

Seinfeld, J. H., and Pandis, S. N.: Atmospheric chemistry and physics : from air pollution to climate change, 2006.

Shen, Y., Virkkula, A., Ding, A., Wang, J., Chi, X., Nie, W., Qi, X., Huang, X., Liu, Q., Zheng, L., Xu, Z., Petäjä, T., Aalto, P. P., Fu, C., and Kulmala, M.: Aerosol optical properties at SORPES in Nanjing, east China, Atmospheric Chemistry and Physics, 18, 5265-5292, doi:10.5194/acp-18-5265-2018, 2018.

Tanré, D., Remer, L. A., Kaufman, Y. J., Mattoo, S., Hobbs, P. V., Livingston, J. M., Russell, P. B., and Smirnov, A.: Retrieval of aerosol optical thickness and size distribution over ocean from the MODIS airborne simulator during TARFOX, Journal of Geophysical Research: Atmospheres, 104, 2261-2278, doi:10.1029/1998jd200077, 1999.

Thalman, R., and Volkamer, R.: Temperature dependent absorption cross-sections of O_2-O_2 collision pairs between 340 and 630 nm and at atmospherically relevant pressure, Physical chemistry chemical physics : PCCP, 15, 15371-15381, doi:10.1039/c3cp50968k, 2013.

Viana, M., Pey, J., Querol, X., Alastuey, A., de Leeuw, F., and Lukewille, A.: Natural sources of atmospheric aerosols influencing air quality across Europe, The Science of the total environment, 472, 825-833, doi:10.1016/j.scitotenv.2013.11.140, 2014.

Wagner, T., Dix, B., Friedeburg, C. v., Frieß, U., Sanghavi, S., Sinreich, R., and Platt, U.: MAX-DOAS O4measurements: A new technique to derive information on atmospheric aerosols-Principles and information content, Journal of Geophysical Research: Atmospheres, 109, D22205, doi:10.1029/2004jd004904, 2004.

Wang, S., Cuevas, C. A., Frieß, U., and Saiz-Lopez, A.: MAX-DOAS retrieval of aerosol extinction properties in Madrid, Spain, Atmos. Meas. Tech., 9, 5089-5101, doi: 10.5194/amt-9-5089-2016, 2016.

Wang, Z., Huang, X., and Ding, A.: Dome effect of black carbon and its key influencing factors: a one-dimensional modelling study, Atmospheric Chemistry and Physics, 18, 2821-2834, doi:10.5194/acp-18-2821-2018, 2018.

Weinzierl, B., Sauer, D., Esselborn, M., Petzold, A., Veira, A., Rose, M., Mund, S., Wirth, M., Ansmann, A., Tesche, M., Gross, S., and Freudenthaler, V.: Microphysical and optical properties of dust and tropical biomass burning aerosol layers in the Cape Verde region an overview of the airborne in situ and lidar measurements during SAMUM-2, Tellus B: Chemical and Physical Meteorology, 63, 589-618, doi:10.1111/j.1600-0889.2011.00566.x, 2017.

Wilcox, E. M., Thomas, R. M., Praveen, P. S., Pistone, K., Bender, F. A., and Ramanathan, V.: Black carbon solar absorption suppresses turbulence in the atmospheric boundary layer, Proceedings of the National Academy of Sciences of the United States of America, 113, 11794-11799, doi:10.1073/pnas.1525746113, 2016.

Wittrock, F., Oetjen, H., Richter, A., Fietkau, S., Medeke, T., Rozanov, A., and Burrows, J. P.: MAX-DOAS measurements of atmospheric trace gases in Ny-Alesund - Radiative transfer studies and their application, Atmospheric Chemistry and Physics, 4, 955-966, 2004.

Xing, C., Liu, C., Wang, S., Chan, K. L., Gao, Y., Huang, X., Su, W.,Zhang,C.,Dong,Y.,andFan,G.:Observationsofthevertical distributions of summertime atmospheric pollutants and the corresponding ozone production in Shanghai, China, Atmos. Chem. Phys., 17, 14275–14289, doi.org/10.5194/acp-17-14275-2017, 2017.

Yoon, S.-C., and Kim, J.: Influences of relative humidity on aerosol optical properties and aerosol radiative forcing during ACE-Asia, Atmospheric Environment, 40, 4328-4338, doi:10.1016/j.atmosenv.2006.03.036, 2006.

Yu, X., Zhu, B., Yin, Y., Yang, J., Li, Y., and Bu, X.: A comparative analysis of aerosol properties in dust and haze-fog days in a Chinese urban region, Atmospheric Research, 99, 241-247, doi:10.1016/j.atmosres.2010.10.015, 2011.

Yu, X., Kumar, K. R., Lu, R., and Ma, J.: Changes in column aerosol optical properties during extreme haze-fog episodes in January 2013 over urban Beijing, Environmental pollution, 210, 217-226, doi:10.1016/j.envpol.2015.12.021, 2016.

Zheng, G. J., Duan, F. K., Su, H., Ma, Y. L., Cheng, Y., Zheng, B., Zhang, Q., Huang, T., Kimoto, T., Chang, D., Pöschl, U., Cheng, Y. F., and He, K. B.: Exploring the severe winter haze in Beijing: the impact of synoptic weather, regional transport and heterogeneous reactions, Atmospheric Chemistry and Physics, 15, 2969-2983, doi:10.5194/acp-15-2969-2015, 2015.